Acta metall. mater. Vol. 40, No. 10, pp. 2639–2649, 1992
Printed in Great Britain. All rights reserved

0956-7151/92 $5.00 + 0.00
Copyright © 1992 Pergamon Press Ltd

PLANE-STRAIN, BUCKLING-DRIVEN DELAMINATION OF THIN FILMS: MODEL EXPERIMENTS AND MODE-II FRACTURE

M. D. THOULESS[1], J. W. HUTCHINSON[2] and E. G. LINIGER[1]

[1]IBM Research Division, T. J. Watson Research Center, Yorktown Heights, NY 10598
and [2]Division of Applied Sciences, Harvard University, Cambridge, MA 02138, U.S.A.

(Received 17 February 1992)

Abstract—A series of model experiments have been conducted to compare observations on buckling-driven delamination of thin films under plane-strain compression with an existing analysis. The results are consistent within the range considered by the theory, which applies when the delamination crack is open to the tip. However, the observations indicate that delamination can occur beyond this range, when the crack tip is closed and undergoing mode-II advance. The theory was extended to incorporate the effect of a contact region in which frictional effects shield the crack tip. A comparison of the analysis with the data indicates that the frictional stress required to explain the apparent toughness observed in this regime is larger than the shear yield strength of the interface. It is inferred that large-scale plasticity may have a significant effect on the results, but this effect has not been included in the analysis.

Résumé—Une série d'expériences modèles ont été effectuées pour comparer des observations sur la délamination due au gauchissement de films minces en compression par déformation plane, aux analyses existantes. Les résultats sont en accord dans le domaine considéré par la théorie qui s'applique lorsque la fissure de délamination est ouvert à l'extrêmité. Cependant, les observations montrent que la délamination peut se produire au delà de ce domaine, lorsque l'extrêmité de la fissure est fermée et subit une progression de mode II. La théorie est généralisée afin d'incorporer l'effet d'une région de contact dans laquelle les effets de frottement ont un effet d'écran sur l'extrêmité de la fissure. La comparaison de cette analyse avec les données indique que la contrainte de frottement requise pour expliquer la ténacité apparente observée dans ce régime est plus grande que la limite élastique en cission de l'interface. On en déduit que la plasticité à grande échelle peut avoir un effet significatif sur les résultats, mais cet effet n'a pas été inclus dans notre analyse.

Zusammenfassung—Mit einer Reihe von Modellexperimenten werden Beobachtungen der durch Verbiegen verursachten Delamination dünner Filme unter Bedingungen ebener Kompression mit einem bestehenden Analyseverfahren verglichen. Die Ergebnisse sind konsistent innerhalb des von der Theorie abgedeckten Bereiches, der die Öffnung des Delaminationsrisses bis zur Spitze betrifft. Allerdings weisen die Beobachtungen darauf hin, daß auch außerhalb dieses Bereiches Delamination auftreten kann; hierbei ist die Rißspitze geschlossen und schreitet in Mode II fort. Die Theorie wird erweitert, um den Einfluß eines Kontaktbereiches zu erfassen, bei dem Reibungseffekte die Rißspitze abschirmen. Vergleich der Analyse mit den Messungen zeigt, daß die zur Erklärung der scheinbaren Zähigkeit in diesem Bereich benötigte Reibungsspannung größer ist als die Fließfestigkeit der Grenzfläche. Es muß also unterstellt werden, daß ausgedehnte Plastizität das Ergebnis beträchtlich beeinflußt; dieser Effekt ist allerdings nicht in der vorgelegten Analyse enthalten.

I. INTRODUCTION

A film that is bonded to a substrate and subjected to a compressive stress may delaminate by a mechanism involving buckling [1–6]. An interface crack can be driven by the stored elastic energy of the system which is released when the film buckles. A companion paper has discussed the effect of biaxial compression on the mechanics of delamination [7]; in the present paper, attention is focused on the plane problem illustrated in Fig. 1. If the interface between a semi-infinite substrate and an elastically isotropic film of thickness h, modulus E and Poisson's ratio ν contains a strip of delamination of width $2b$, then classical buckling theory predicts that, in plane-strain, the stress required to buckle the film above the flaw is

$$\sigma_c = \pi^2 E(h/b)^2[12(1-\nu^2)]^{-1}. \quad (1)$$

A driving force for delamination develops when the magnitude of the compressive stress within the film, $-\sigma_0$, is larger than this value. A general relationship between this energy-release rate, $\mathcal{G}$, and the buckling parameter $\Sigma = \sigma_0/\sigma_c$ can be expressed as [1, 3, 10]

$$\mathcal{G} = \mathcal{G}_0(1 - 1/\Sigma)(1 + 3/\Sigma) \quad (2)$$

where $\mathcal{G}_0$ is the elastic energy per unit area of the unbuckled film

$$\mathcal{G}_0 = (1-\nu^2)h\sigma_0^2/2E. \quad (3)$$

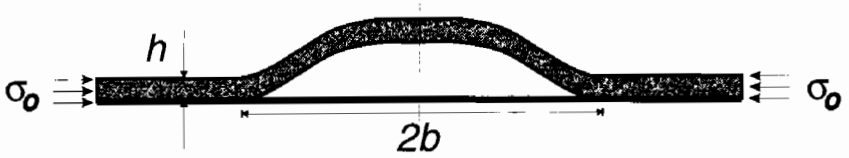

Fig. 1. Schematic illustration of the plane problem considered in this paper.

The interface crack associated with this geometry is subject to mixed-mode conditions [8–10]. For example, if the film and substrate have the same elastic properties, and the stress in the film is uniform, Hutchinson and Suo [10] have calculated the ratio between the mode-II and mode-I stress-intensity factors as

$$K_{II}/K_I = \tan\psi = \frac{2 + (\sigma_0/\sigma_c - 1)^{1/2}\tan\omega}{-2\tan\omega + (\sigma_0/\sigma_c - 1)^{1/2}} \quad (4)$$

where ψ is termed the phase angle of loading, and ω is 52.1°. From this expression it can be seen that when buckling just occurs, at $\Sigma = 1$, the mode-I and mode-II components are almost equal with $\psi = -37.9°$. An increase in Σ, which can result either from an increased stress or from growth of the delamination, causes ψ to decrease until, at $\Sigma = 7.6$, it equals $-90°$ and the crack is under conditions of pure mode-II.

The change in ψ as the delamination spreads has a profound influence on the fracture behaviour of such a system. In general, the fracture resistance of an interface, Γ, varies with the ratio K_{II}/K_I [11–14]. While there appears to be no unique relationship, Γ frequently appears to increase with the proportion of mode-II. Therefore, as the delamination spreads under a buckling film, the fracture resistance of the interface can be expected to increase. A close inspection of equation (2) shows that, if this is not the case, an interface crack will spread without limit once it begins to propagate except under special conditions [3]. When Γ increases with ψ, growth of the crack to a stable size is much more likely, as can be illustrated by assuming a relationship between the two parameters. For example, one empirical relationship that appears to capture some of the essential elements of experimentally observed mixed-mode fracture resistances is

$$\Gamma(\psi) = \Gamma_{Ic}[1 + \tan^2(1-\lambda)\psi] \quad (5)$$

where Γ_{Ic} is the fracture resistance under pure mode-I conditions, and λ is a fitting parameter in the range (0, 1). If this relationship is combined with equations (2), (3) and (4), and with the condition that delamination cannot occur if

$$\mathcal{G} < \Gamma(\psi) \quad (6)$$

it is possible to predict the delamination behaviour as a function of the geometrical parameters, elastic constants, and the stress in the film. This is illustrated in Fig. 2. The curves in this figure were obtained by equating $\mathcal{G}$ in equation (2) to $\Gamma(\psi)$ in equation (5). Below the curves, delamination is not possible; it is possible above them. The dashed line illustrates a hypothetical trajectory for the relevant parameters as the stress in the film is increased. The initial portion of this trajectory (AB) is a straight line through the origin with a slope inversely related to the original defect size; it represents an increase in stress while the flaw size remains constant. The film buckles when $\sigma_0/\sigma_c = 1$, but no delamination occurs. Between B and C, delamination can occur at a constant stress; the trajectory is then a line parallel to the x-axis. In a truly rate-independent system, the delamination from B to C would take place dynamically. For this particular example, no further delamination is possible once point C has been reached no matter how much further the stress is increased. However, depending on the initial flaw size and on the value of λ, it is possible to reach regions in which delamination progresses in a stable fashion as the magnitude of the stress is increased.

This paper consists of two parts. In the first part, the results of some model experiments that were designed to explore the phenomenon of delamination by buckling are described. In the second part, some additional theoretical work that was prompted by some of the observations made during the course of the experiments is presented. In particular, the theory has been expanded to explore the role of the contact zone that must exist behind the crack tip when $\sigma_0/\sigma_c > 7.6$.

2. EXPERIMENTS

The system chosen for study consisted of thin mica sheets bonded to a mild steel substrate by means of

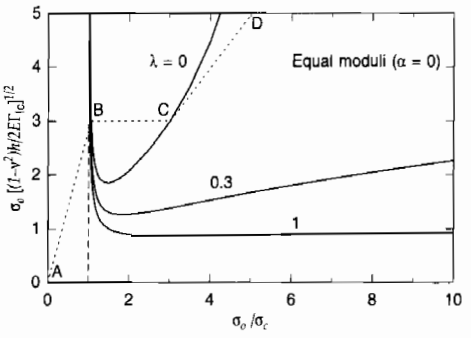

Fig. 2. A plot illustrating the conditions under which delamination can occur for different mixed-mode failure criteria.

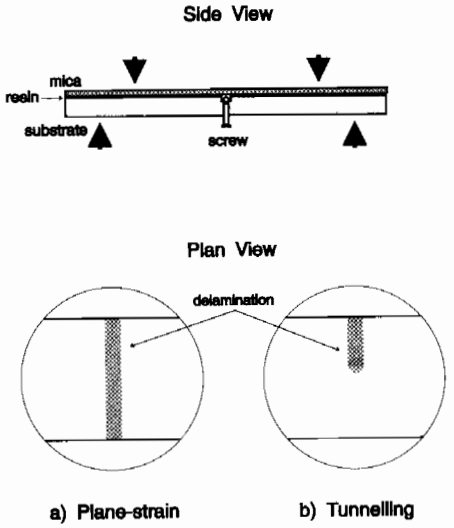

Fig. 3. The configuration used for the experiments described in this paper.

a brittle thermoplastic resin† (Fig. 3). Mica was chosen for the film because it provided a film of controlled thickness which was elastic and could be obtained in sheets thin enough to be suitably flexible for the experiments. Several thicknesses of mica, ranging from 30 to 120 μm, were used in these experiments. Mild steel was selected as a substrate material so as to approximate conditions in which the elastic constants of the film and substrate are equal. (If values for Young's modulus of mica‡ and steel are taken to be 172 and 196 GPa respectively, and the respective Poisson's ratios are assumed to be about 0.2 and 0.3, the Dundurs' parameters measuring the elastic mismatch in plane strain are $\alpha \simeq 0.09$ and $\beta \simeq 0.06$.)

It should be noted that a thermoplastic resin was used in these experiments, so that, owing to the difference in thermal expansion between mica and steel, the mica was under a residual stress at room temperature. To establish the magnitude of this stress, a measurement of the temperature at which the resin set, and below which elastic stresses could develop, was required. This temperature was determined to be 52 ± 2°C by using the resin to bond a sheet of mica to a fused-silica wafer and measuring the curvature of the composite system at room temperature (22°C) using optical interferometry. Consequently, by using values of 8.1×10^{-6}/°C and 17.3×10^{-6}/°C for the thermal expansions of mica‡ and steel respectively, it was calculated that there was a residual compressive stress of 59 ± 4 MPa in the mica at room temperature. This stress had to be added to the applied stress to determine the total compressive stress acting on the mica.§

The specimens were in the form of composite beams of width 25 mm, depth 6 mm, and an inner-span length (where the delamination occurred) of 45 mm. An initial flaw could be introduced into the interface in a controlled fashion by means of screws threaded through the substrate to rest against the underside of the mica (Fig. 3). Once the flaw was created, the screws were removed. The experiments consisted of measuring the length of the delamination and loading the sample in four-point bending under displacement-controlled conditions. The load, and hence the applied stress in the mica, at which the flaw propagated was noted, and the experiment repeated with this new flaw. These measurements were continued until the delamination reached the inner loading points. In all cases the interface crack occurred between the mica and the adhesive layer.

In one set of experiments, the initial delamination extended across the entire width of the specimen, so as to ensure plane-strain conditions. Experimental data relating the stress in the film to the buckling parameter, Σ, are presented in Fig. 4. For the thicker films, the data appear to fall into two distinct groups: points associated with propagation, and points associated with arrest of the interface crack. These points are represented by open and closed symbols respectively. If the value of $\mathcal{G}$ at which arrest or propagation of the crack occurs is taken to be the fracture resistance of the interface, equations (2) and (3) can be used to re-plot the data as this apparent fracture resistance against σ_0/σ_c (Fig. 5).¶

Finally, for the data in the range $1 \leqslant \sigma_0/\sigma_c \leqslant 7.6$, equation (4) can be used to plot the dependence of the apparent fracture resistance on the nominal phase angle (ignoring any elastic inhomogeneities) (Fig. 6). Empirical fits to equation (5) were determined for this system; these are also shown in Fig. 6. For this particular combination of materials, it appears that while $\lambda \simeq 0.3$ gave a good fit for all the data, there was considerable variation in the estimated values of Γ_{Ic}. For example, it is evident that the difference in the conditions required to propogate the delamination and those required to arrest it can be associated with a difference in Γ_{Ic} for the two events. It appeared to be more difficult to start the crack then to keep it moving. The measured fracture resistance also depended on the thickness of the mica. This was probably a consequence of the finite thickness of the adhesive layer which, being about 10–20 μm, was not insignificant compared to the films. The results cannot, therefore, be regarded as rigorous fracture-mechanics measurements of the fracture resistance; they are clearly not geometry independent. However, it should be emphasised that the sets of data for each

†Buehler Lakeside-80 Thermoplastic Cement.

‡From the manufacturer's data sheet.

§The residual stress state is equi-biaxial, while the additional stresses subsequently induced in the unbuckled film correspond to in-plane plane strain. Nevertheless, with σ_0 denoting the total compressive stress is the film along the axis of the beam (Fig. 3), $\mathcal{G}_0$ defined in equation (3) still represents the strain energy per unit area of unbuckled film which is available when released under plane-strain conditons, and equation (2) continues to apply.

¶Equation (2) is valid even when $\sigma_0/\sigma_c > 7.6$.

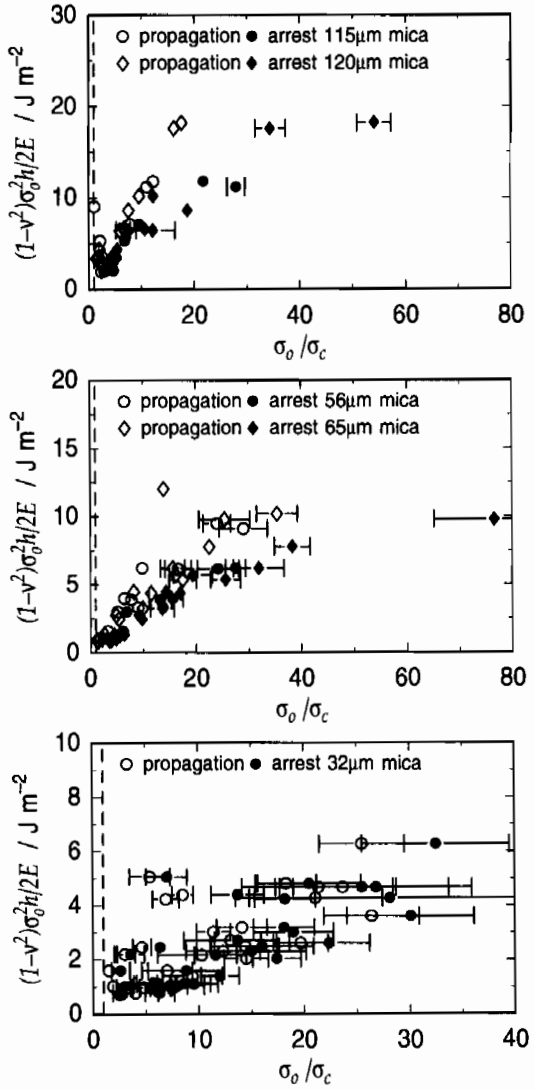

Fig. 4. Experimental data relating the stress in the mica film to the buckling parameter for different film thicknesses.

thickness of mica were obtained using many samples. The observed trends were systematic and reproducible. Furthermore, the values of the fracture resistance correlated well with experimental data obtained for the same system under different loading conditions [7, 16].

In a second set of experiments, the initial delamination was limited to approximately half the width of the beam (Fig. 3). It was observed that two failure mechanisms were possible; either the delamination expanded in width, or it grew from its tip and tunnelled across the specimen. The plot of Fig. 7 shows the experimental conditions under which these two mechanisms occurred, and compares them with the observations for plane-strain growth. It can be seen from this figure that the first type of behaviour was limited to narrow delaminations when σ_0/σ_c was less than about four. Tunnelling occurred at larger values of the buckling parameter. Typically, a small defect would initially increase in width then, at some critical size, a transition would occur and the delamination would start to grow across the beam. Once tunnelling occurred, no further increase in the width was observed until the delamination extended across the entire sample and plane-strain conditions were restored. The micrographs of Fig. 8 illustrate this behaviour by showing various stages of development for such a delamination. It is, perhaps, of interest to emphasise one further observation: the width of the tunnelling region was approximately constant and independent of the width of the initial defect. A small defect would grow to approximately the transition size; in a large defect, a "nose" would develop and grow at the tip of the delamination region.

A theoretical treatment of tunnelling is given by Hutchinson and Suo [10], and the predicted behaviour for $\lambda = 0.3$ is shown in Fig. 9. The tunnelling analysis applies strictly only to the steady-

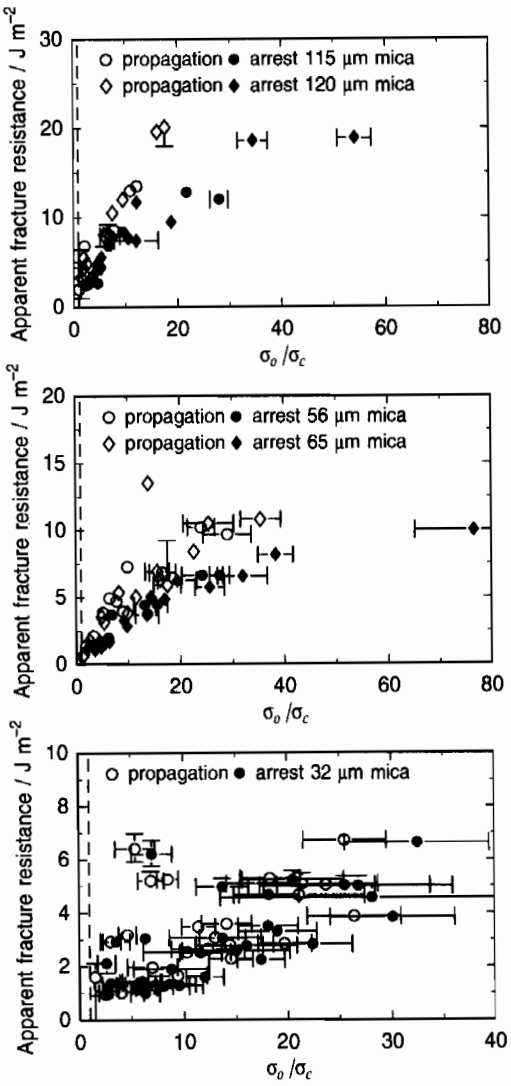

Fig. 5. Apparent fracture resistance plotted as a function of the buckling parameter.

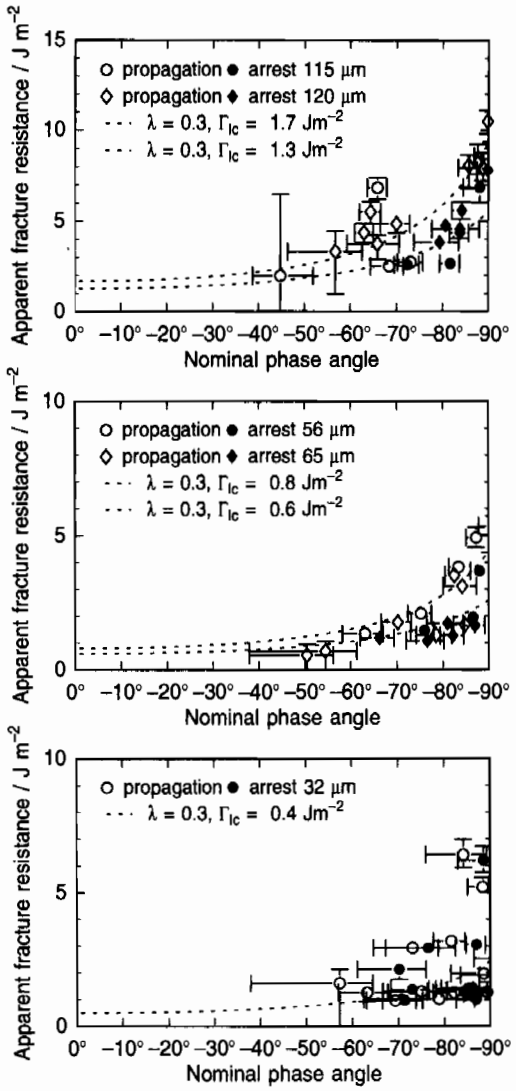

Fig. 6. A plot of the dependence of the apparent fracture resistance on the nominal phase angle.

state propagation of a blister under the assumption that its width has already been established. Additionally, the analysis was carried out for conditions of equi-biaxial stress in the unbuckled film, but the predictions are not expected to have a strong dependence on the component of stress in the film acting parallel to the tunnelling direction. The main features seen in Fig. 9 closely reflect the experimental observations reported above. Namely, for σ_0/σ_c below about 5, expansion in the width of the blister rather than tunnelling is predicted; conversely, for σ_0/σ_c above this transition, tunnelling is predicted. The comparison between theory and experiment is very satisfactory.

3. THE ROLE OF CONTACT ON MODE-II INTERFACE CRACK GROWTH

As discussed in Section 2, contact must occur behind the tip of an interface crack when the buckling parameter exceeds 7.6 and negligible elastic mismatch is assumed. The tip is then in pure mode-II. However, it is evident from the experimental data of Fig. 5, that shielding of the crack tip must be occurring in this range of σ_0/σ_c. If no shielding were occurring, the apparent fracture resistance of the interface would be constant; in contrast, the data shows a systematic increase with σ_0/σ_c.

This section examines the role of a contact zone on mode-II crack growth along an interface. It is divided into three subsections: the first deals with the basic solution for a frictional contact zone behind an interface-crack tip, the second couples this edge-crack solution to the buckled-blister solution, and the last compares the theory and experiments. Comparison of the predictions of the analysis with the data in Section 2 suggests that an additional contribution to shielding other than friction must be present, probably large-scale plastic yielding in the adhesive.

3.1. Basic edge-crack solution

When the crack is open all the way to the tip (i.e. $d = 0$, in Fig. 10), the stress intensity factors are given by [15]

$$K_I = -0.434Sh^{1/2} + 1.934Mh^{-3/2}$$
$$K_{II} = -0.558Sh^{1/2} - 1.503Mh^{-3/2} \quad (7)$$

where S is the average tensile-stress *change* in the film, and M is the moment (per unit length of crack front) acting in the film at the crack edge. The energy-release rate made available by the buckled film is

$$\mathcal{G} = [(1-\nu^2)h/2E][S^2 + 12(M/h^2)^2]. \quad (8)$$

This equals the energy-release rate at the tip when the crack tip is not shielded, i.e.

$$\mathcal{G} = \mathcal{G}_{tip} \equiv [(1-\nu^2)/E](K_I^2 + K_{II}^2). \quad (9)$$

Equations (7) and (8) satisfy this relation.

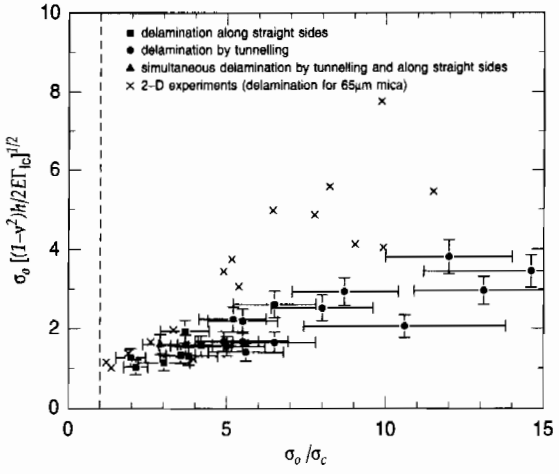

Fig. 7. Experimental results showing the transition between the mechanisms of tunnelling and width increase for a blister in a 0.065 μm mica film. The plane-strain data have been included to provide a comparison of the relative energies required for each mechanism.

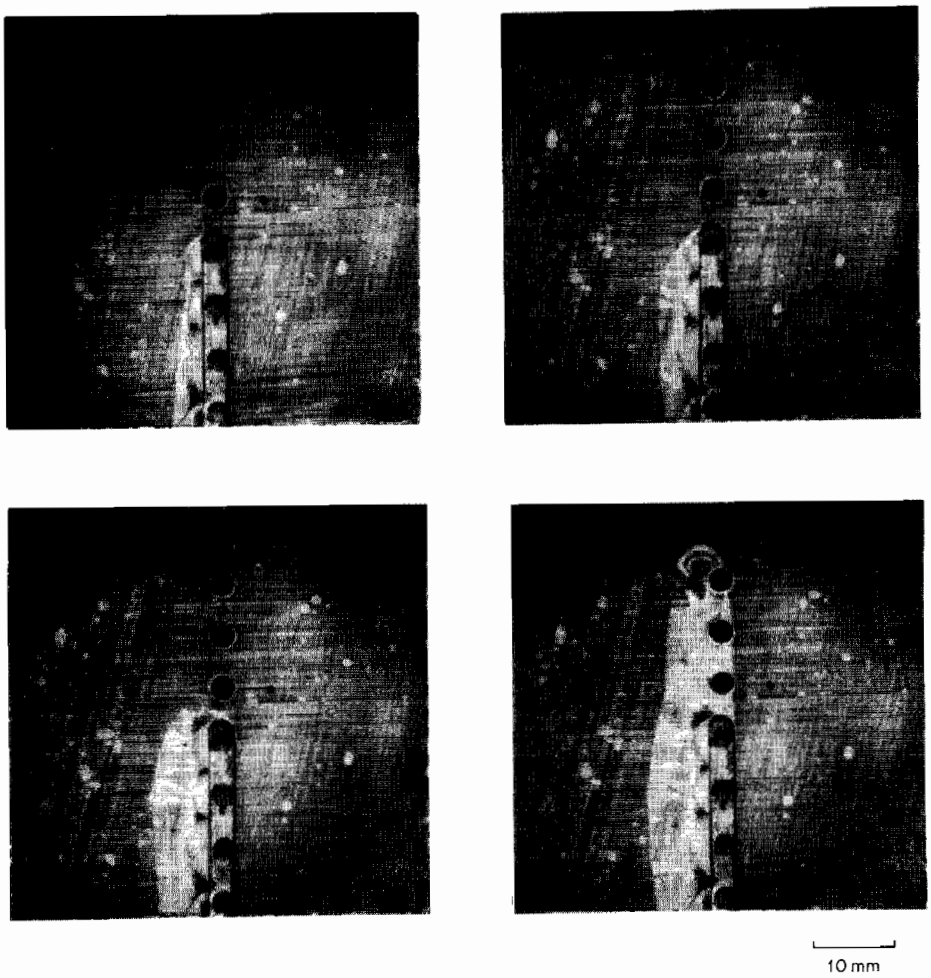

Fig. 8. A series of micrographs showing the development of a defect of finite length, and the transition in growth mechanism.

Equation (7) implies that $K_I > 0$ and, hence, that the crack is open all the way to the tip if $M/(Sh^2) > 0.224$. Conversely, however, when $M/(Sh^2) < 0.224$, contact of the crack surfaces must occur immediately behind the tip. Under these conditions, the energy-release rate at the tip is

$$\mathcal{G}_{tip} = [(1 - \nu^2)/E]k_{II}^2 \qquad (10)$$

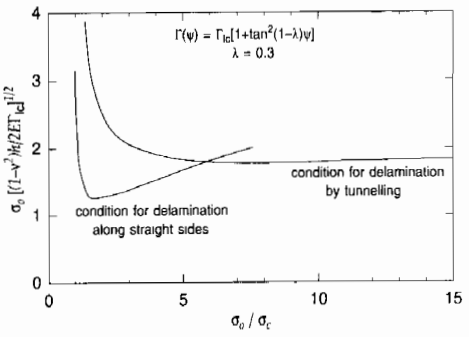

Fig. 9. Theoretical plot showing energy-release rates for mechanisms of tunnelling and width increase for a blister ($\lambda = 0.3$).

where k_{II} is the local mode-II stress-intensity factor at the crack tip. The total energy-release rate $\mathcal{G}$ made available by the buckled film is still given by equation (8) [or equivalently, by equation (2)]. Any difference between $\mathcal{G}$ and $\mathcal{G}_{tip}$ is absorbed by resistive shear stresses in the contact zone.

The details of an analysis which assumes a *constant friction stress* $\sigma_{xy} = -\tau$ acting over the contact region is given in the Appendix (Fig. 10). A summary of the results are shown in Fig. 11 in which the shielding factor, $\mathcal{G}_{tip}/\mathcal{G}$, and the length of the contact region are plotted as functions of M/Sh^2 and τ/S. It will be noted that, for a fixed τ/S, the contact region increases with decreasing M/Sh^2

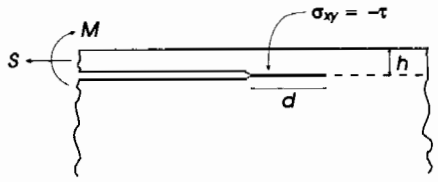

Fig. 10. Schematic illustration of a delamination crack with a contact zone of length d behind the crack tip.

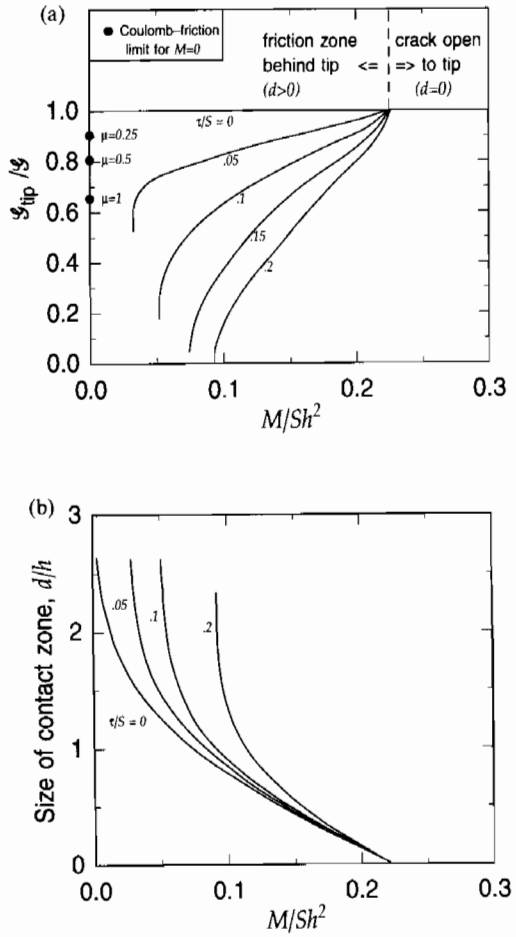

Fig. 11. Plots of (a) the shielding factor, and (b) the contact-zone length as functions of M/Sh^2 for the general edge-crack problem in which the shear resistance, τ, is assumed to be constant within the contact zone.

while $\mathcal{G}_{tip}/\mathcal{G}$ decreases. Depending on the value of τ/S, there is a lower limit to M/Sh^2 when the contact zone becomes so large that the crack tip "locks up", i.e $\mathcal{G}_{tip}/\mathcal{G} \to 0$.

Included in Fig. 11(a) are some values for the shielding factor in the limit $M = 0$ when Coulomb friction is assumed to act in the contact region. The results are taken from a recent analysis by Stringfellow and Freund [17]; these authors assumed the friction stress in the contact zone was given by $\tau = \mu\sigma_{yy}$, where $-\sigma_{yy}$ is the compressive stress acting across the debonded interface. It can be seen that, even in the limit $M = 0$ and with a coefficient of Coulomb friction of unity, $\mathcal{G}_{tip}/\mathcal{G}$ is only reduced to about 0.6†. To explain the data of Fig. 4, shielding factors as low as about 0.2 must be invoked. It was for this reason that no attempt was made to compute the dependence of $\mathcal{G}_{tip}/\mathcal{G}$ on M/Sh^2 for a Coulomb-friction zone, and an alternative to the Coulomb-friction characterisation was sought. Owing to the inability of the Coulomb-friction assumption to capture experimental trends for fibre debonding and pullout or pushout in fibre-reinforced, brittle-matrix composites, alternative characterisations for friction have also been used to model these problems [18, 19]. A constant friction stress τ, which is independent of the normal compression acting across the debonded interface in the contact region, appears to be more successful at reproducing some of the experimental behaviour, although the physical basis of this characterisation is poorly understood.

†The influence of elastic mismatch is also determined in [17], but the mica/steel system is well represented by the approximation of no mismatch.

3.2. Coupling of the edge-crack solution to the Euler solution for the buckled film

The buckled film is modelled as a wide Euler column of length $2b$ which is clamped along its ends. The moment and average in-plane stress change at the edge of the clamped buckled plate are identified with the corresponding quantities, M and S, of the edge-crack problem. Provided that b is large compared to both h and d, and $\sigma_0/\sigma_c > 1$, M and S, can be related to the stress in the unbuckled film by [10]

$$M = \frac{\pi^2 E h^4}{24(1-\nu^2)b^2}\left[\frac{4}{3}\left(\frac{\sigma_0}{\sigma_c} - 1\right)\right]^{1/2} \tag{11}$$

and

$$S = \sigma_0 - \sigma_c = \frac{\pi^2 E h^2}{12(1-\nu^2)b^2}\left[\frac{\sigma_o}{\sigma_c} - 1\right]. \tag{12}$$

So that

$$\frac{M}{Sh^2} = \frac{1}{\sqrt{3}}\left[\frac{\sigma_0}{\sigma_c} - 1\right]^{-1/2} \tag{13}$$

where σ_c is given by equation (1). The energy-release rate made available by the buckled film is given by equation (8), which upon substitution of equations (11) and (12) becomes equation (2). From equation (13), it follows that $M/Sh^2 = 0.224$ when $\sigma_0/\sigma_c = 7.6$, and is reduced to 0.092 when $\sigma_0/\sigma_c = 40$ which corresponds to the upper limit of most of the data represented in Fig. 4.

To summarise: when σ_0/σ_c is greater than 7.6, the crack tip is in pure mode-II with a contact region of width d, while $\mathcal{G}$ is still given by equation (2). If a constant friction stress, τ, acts over the contact region, the ratio $\mathcal{G}_{tip}/\mathcal{G}$ can be obtained either from Fig. 11(a) or from the information given in the Appendix. A non-dimensionalisation of the equations reveals that $\mathcal{G}_{tip}/\mathcal{G}$ depends only on σ_0/σ_c and one other parameter: τ/σ_R, where σ_R is a reference quality with dimensions of stress defined by

$$\sigma_R = \left[\frac{2E\mathcal{G}_{tip}}{(1-\nu^2)h}\right]^{1/2}. \tag{14}$$

Curves of $\mathcal{G}/\mathcal{G}_{tip}$ vs σ_0/σ_c are plotted in Fig. 12 for various values of τ/σ_R. Appreciable shielding occurs only when τ/σ_R is greater than about 0.1.

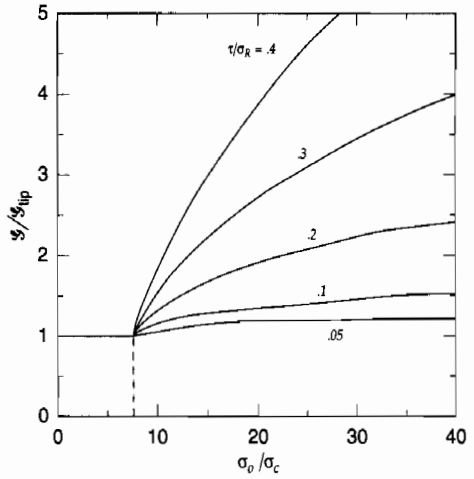

Fig. 12. Plot of $\mathscr{G}/\mathscr{G}_{tip}$ as functions of σ_0/σ_c and the normalised friction stress, τ/σ_R.

3.3. *Interpretation of theory and experiment*

In making a comparison between the theory and the experiments, it is assumed that fracture occurs when $\mathscr{G}_{tip} = \Gamma(-90°)$ for $\sigma_0/\sigma_c > 7.6$; in other words, the mode-II toughness controls advance of the actual crack tip. Furthermore, as a working hypothesis, the mode-II interface toughness, $\Gamma(-90°)$, is taken as the value of $\mathscr{G} \equiv \mathscr{G}_{tip}$ required for fracture when $\sigma_0/\sigma_c = 7.6$. The trends of the experimental data shown in Fig. 5 are consistent with the theoretical curve in Fig. 12 associated with a value of τ/σ_R of about 0.3, i.e. a friction stress of

$$\tau \approx 0.3\left[\frac{2E\Gamma(-90°)}{(1-\nu^2)h}\right]^{1/2}. \qquad (15)$$

From the data in Fig. 6, a value of 8 J m^{-2} can be assigned to $\Gamma(-90°)$ for the film/substrate systems with $h = 120\,\mu$m, 4 J m^{-2} for $h = 65\,\mu$m, and 3 J m^{-2} for $h = 32\,\mu$m. The representative values of τ computed from equation (15) are 47 MPa, 46 MPa and 56 MPa. These stress levels are about a factor two greater than the shear yield strength of the adhesive, as measured by a hardness test, and are certainly much too large to be attributed solely to frictional processes.

The estimates of the shear yield strength of the adhesive indicate that large-scale plasticity may be significant at the large values of σ_0/σ_c. Equation (10) and the values of $\Gamma(-90°)$ given by the data in Fig. 6 suggest that $k_{II} \simeq 1$ MPa$\sqrt{\text{m}}$ for crack advance to occur. If the stresses remain elastic, the shear stress on the interface at a distance r ahead of the crack tip is given by

$$\sigma_{xy} = \frac{k_{II}}{\sqrt{2\pi r}}. \qquad (16)$$

So, at a distance of 100 μm the shear stress would be about 40 MPa. Although this is a fairly rough estimate, it does appear that the shear stress on the interface exceeds the yield strength of the adhesive in shear at a distance comparable to, or greater than, the film thickness. Therefore, at least in this particular system, large-scale plasticity may be playing a role. Such effects have not been taken into account in the present model.

4. CONCLUSIONS

Experimental observations on buckling-driven delamination of thin films showed excellent agreement with a previous analysis of the phenomenon. However, the experiments illustrated the necessity of extending the theory to accommodate the possibility of crack propagation occurring when the crack tip is closed. A similar phenomenon occurs when a film under a residual compression delaminates from an edge crack (Fig. 13). When the crack in such a system is long compared to the film thickness, the mechanics is identical to that of buckling-driven delamination in the limit $\sigma_0/\sigma_c \to \infty$. As a test of the consistency between different experimental configurations, an additional experiment was performed in which a strip† of mica was bonded to an aluminium substrate, an edge crack introduced by means of a razor blade into the interface between the film and substrate, and the sample cooled until the delamination propagated. The thermal-expansion mismatch between the aluminium and the mica induced an equi-biaxial, compressive stress, $-\sigma^*$, in the mica. The energy-release rate for a crack in the interface is

$$\mathscr{G} = (1-\nu)h\sigma_*^2/E. \qquad (17)$$

For a mica film 140 μm thick, catastrophic delamination occurred when this reached a value of 17 ± 3 J m^{-2}. This is in excellent agreement with the apparent fracture resistance of the same interface obtained for the more extreme values of σ_0/σ_ϵ in the buckling-driven delamination experiments.

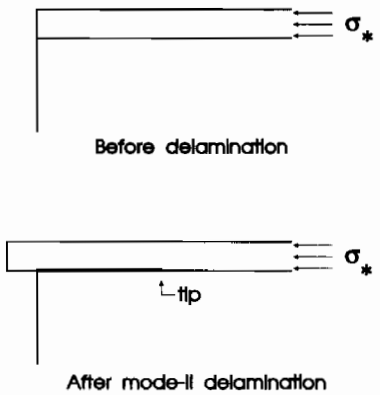

Fig. 13. Schematic illustration of delamination from an edge crack under a film with a residual compressive stress.

†Wide films tended to fail by the development of crack-front instabilities of the type described in Ref. [7].

It remains an important issue as to how to model a mode-II interface crack in the presence of a contact zone. In this paper it has been assumed that propagation is controlled by the mode-II toughness $\Gamma(\pm 90°)$ at the tip, with shear tractions in the contact region shielding the crack tip from the applied $\mathcal{G}$. This is a natural extension of modelling mixed-mode fracture when $K_1 > 0$ [20]. A comparison with the experimental data showed that an assumption of Coulomb friction in the contact region could not account for the dramatic increase in the observed fracture resistance of the interface. A model which invoked a constant shear strength for the interface was capable of reproducing the observations; however, the required shear strength was approximately twice the measured shear yield strength of the adhesive used in the interface. It appears that, in this system at least, large-scale plasticity effects are likely to be important, and these effects have not been incorporated in the present analysis.

Acknowledgements—The work of JWH was supported in part by grants NSF-MSS-90-20141 and NSF-DMR-89-20490, and in part by the Division of Applied Sciences, Harvard University.

REFERENCES

1. H. Chai, C. D. Babcock and W. G. Knauss, *Int. J. Solid Struct.* **17,** 1069 (1981).
2. D. Nir, *Thin Solid Films* **112,** 41 (1984).
3. G. Gille, *Current Topics in Materials Science*, Vol. 12, Chap. 7, pp. 420–472. North Holland, Amsterdam (1985).
4. A. G. Evans and J. W. Hutchinson, *Int. J. Solid Struct.* **20,** 455 (1984).
5. A. S. Argon, V. Gupta, H. S. Landis and J. A. Cornie, *J. Mater. Sci.* **24,** 1207 (1989).
6. G. A. J. Amaratunga and M. E. Welland, *J. appl. Phys.* **68,** 5140 (1990).
7. J. W. Hutchinson, M. D. Thouless and E. G. Liniger, *Acta metall. mater.* **40,** 295 (1992).
8. J. D. Whitcomb, *Composite Sci. Technol.* **25,** 19 (1986).
9. H. Chai, *Int. J. Fract.* **46,** 237 (1990).
10. J. W. Hutchinson and Z. Suo, *Advances in Applied Mechanics* (edited by J. W. Hutchinson and T. Y. Wu), pp. 63–191. Academic Press, Amsterdam (1992).
11. H. C. Cao and A. G. Evans, *Mech. Mater.* **7,** 295 (1989).
12. M. D. Thouless, *Acta metall. mater.* **38,** 1135 (1990).
13. J. S. Wang and Z. Suo, *Acta metall. mater.* **38,** 1279 (1990).
14. K. M. Liechti and Y.-S. Chai, *J. appl. Mech.*, in press.
15. M. D. Thouless, A. G. Evans, M. F. Ashby and J. W. Hutchinson, *Acta metall.* **35,** 1333 (1987).
16. H. M. Jensen and M. D. Thouless, *Int. J. Solid Struct.*, to be published.
17. R. G. Stringfellow and L. B. Freund, *Int. J. Solid Struct.*, to be published.
18. D. B. Marshall, M. C. Shaw and W. L. Morris, *Acta metall. mater.*, **40,** 443 (1992).
19. P. D. Warren, T. J. Mackin and A. G. Evans, to be published.
20. A. G. Evans and J. W. Hutchinson, *Acta metall.* **37,** 909 (1989).
21. J. Dundurs, in *Mathematical Theory of Dislocations*, pp. 71–115. ASME, NY (1969).
22. H. Tada, P. C. Paris and G. R. Irwin, *The Stress Analysis of Cracks Handbook* Del Research Corp, St. Louis, Mo. (1985).

APPENDIX

Solution of the Edge-crack Problem with Constant τ

As in Section 3, the Young's modulus and Poisson's ratio of the film and substrate are taken to be E and ν, and plane-strain conditions are assumed. A contact region develops behind the crack tip when $M/(Sh^2) < 0.224$ (cf. Fig. 11). To construct the solution corresponding to the case when a constant friction stress τ acts between the crack surfaces within the contact region, a distribution of dislocations is used to represent the crack-face displacements; integral-equation procedures are then used to solve for these distributions. The procedure used here generalises that employed in [15] and [17].

The film thickness, h, is used to non-dimensionalise the cartesian co-ordinates which are centered at the left end of the contact region (cf. Fig. 11) with the x-axis along the interface and the y-axis as the vertical. The crack tip is at $(d, 0)$. Along $y = 0$ for $x < 0$, $\sigma_{yy} = \sigma_{xy} = 0$ on both faces of the crack and the crack is open. On $y = 0$ for $0 < x < d$, the crack is closed but its faces slide over one another with $\sigma_{xy} = -\tau$ on each face.

The tractions at a point x anywhere along $y = 0$ due to a dislocation with a Burgers vector (b_x, b_y) at $(\xi, 0)$ have the form

$$8\pi(1-\nu^2)\sigma_{xy}/E = 2b_x\zeta^{-1} + b_x F_{xx}(\zeta) + b_y F_{xy}(\zeta) \quad \text{(A1)}$$

$$8\pi(1-\nu^2)\sigma_{yy}/E = 2b_y\zeta^{-1} + b_x F_{yx}(\zeta) + b_y F_{yy}(\zeta) \quad \text{(A2)}$$

where $\zeta = x - \xi$ and the F's are given in [15] and [21].

The components of the crack-face displacements (δ_x, δ_y) are related to the distribution of the dislocations by

$$\delta_x(x) = \int_x^d b_x(\xi)\,\mathrm{d}\xi \quad \text{and} \quad \delta_y(x) = \int_x^0 b_y(\xi)\,\mathrm{d}\xi. \quad \text{(A3)}$$

The representations of the dislocation distributions are given next. Let $t = (1 + \xi - d)/(1 - \xi + d)$ so that the interval $-\infty < \xi \leqslant d$ corresponds to $-1 < t \leqslant 1$. Then let

$$b_x(\xi) = (1-\nu^2)(\tau/E) f_0(\xi) + (1-t)^{-1/2} \sum_{k=1}^{n_1} a_k T_{k-1}(t) \quad \text{(A4)}$$

where $T_k(t)$ is the Chebyshev polynomial of the first kind of degree k, and

$$f_0(\xi) = \frac{8}{\pi}\left\{\left(1 - \frac{\xi}{d}\right)^{-1/2} - \frac{1}{2}\ln\left|\frac{1+\sqrt{1-\xi/d}}{1-\sqrt{1-\xi/d}}\right|\right\}. \quad \text{(A5)}$$

The contribution $(1-\nu^2)(\tau/E)f_0(\xi)$ is the exact distribution [22] for a semi-infinite mode-II crack in an *infinite* plane with crack-surface tractions $\sigma_{yy} = 0$ on $-\infty < x < d$, $\sigma_{xy} = 0$ on $-\infty < x < 0$, and $\sigma_{xy} = -\tau$ on $0 < x < d$. The reason for the incorporation of this term will be mentioned later. Let $s = (1 + \xi)/(1 - \xi)$ so that the interval $-\infty < \xi \leqslant 0$ corresponds to $-1 < s \leqslant 1$, and let

$$b_y(\xi) = [(1-s)^{1/2}/(1+s)] \sum_{k=1}^{n_2} b_k T_{k-1}(s). \quad \text{(A6)}$$

This choice is consistent with the condition that the normal stress is bounded as $x \to 0^+$ and the crack opens smoothly for $x \leqslant 0$.

The integral equations satisfying the boundary conditions on the tractions [when expressed using equations (A4) and (A6)] are

$$\sum_{k=1}^{n_1} a_k \int_{-\infty}^{d} (1-t)^{-1/2} T_{k-1}(t)[2(x-\xi)^{-1} + F_{xx}(x-\xi)]\,d\xi + \sum_{k=1}^{n_2} b_k \int_{-\infty}^{0} [(1-s)^{1/2}/(1+s)] \times T_{k-1}(s) F_{xy}(x-\xi)\,d\xi = -[(1-\nu^2)\tau/E] \times \int_{-\infty}^{d} f_0(\xi) F_{xx}(x-\xi)\,d\xi; \quad -\infty < x < d. \tag{A7}$$

$$\sum_{k=1}^{n_1} a_k \int_{-\infty}^{d} (1-t)^{-1/2} T_{k-1}(t) F_{yx}(x-\xi)\,d\xi + \sum_{k=1}^{n_2} b_k \int_{-\infty}^{0} [(1-s)^{1/2}/(1+s)] \times T_{k-1}(s)[2(x-\xi)^{-1} + F_{yy}(x-\xi)]\,d\xi = -[(1-\nu^2)\tau/E] \int_{-\infty}^{d} f_0(\xi) F_{yx}(x-\xi)\,d\xi; \quad -\infty < x < 0. \tag{A8}$$

Since the term involving $f_0(\xi)$ satisfies the traction conditions exactly on $-\infty < x < d$ for the fully infinite region, the right-hand terms involve only the extra terms associated with the traction-free top surface of the semi-infinite plane. This is a convenient way to "apply" the shear loading τ since the correct logarithmic behaviour in $b_x(\xi)$ near $\xi = 0$ is incorporated in this term. Appended to these equations is the imposed condition

$$-b_x + \frac{1}{2}\frac{db_y}{d\xi} = \frac{(1-\nu^2)S}{E} \quad \text{as} \quad \xi \to -\infty \tag{A9}$$

which follows from the connections that

$$d\delta_y/dx \to \epsilon_x = [(1-\nu^2)/E](S + 6Mh^{-2}) \tag{A10a}$$

along the crack face on the top arm as $x \to -\infty$, and that

$$M = \frac{Eh^3\kappa_\infty}{12(1-\nu^2)} = \frac{-Eh^3}{12(1-\nu^2)}\frac{db_y}{d\xi} \quad \text{as} \quad \xi \to -\infty \tag{A10b}$$

where κ_∞ is the curvature of the arm as $x \to -\infty$.

The set of $n \equiv n_1 + n_2$ unknowns (a_k, b_k), are determined by satisfying equation (A7) at m_1 points for x on $(-\infty, d)$ and equation (A8) at m_2 points for x on $(-\infty, 0)$ where $m_1 + m_2 = n - 1$, with equation (A9) as the remaining equation. Other details of the numerical procedure are similar to the somewhat simpler problem solved in [15]. The local mode-II stress-intensity factor at the crack tip is given by

$$k_{II}h^{-1/2} = \lim_{x\to d}\sqrt{\frac{2\pi}{(d-x)}}\frac{Eb_x}{4(1-\nu^2)} = 2\left(\frac{2d}{\pi}\right)^{1/2}\tau + \frac{\sqrt{\pi}}{4}\frac{E}{(1-\nu^2)}\sum_{k=1}^{n_1} a_k T_{k-1}(1) \tag{A11}$$

while, from equations (A10) and (A6),

$$Mh^{-2} = \frac{E}{12\sqrt{2}(1-\nu^2)}\sum_{k=1}^{n_2} b_k T_{k-1}(-1). \tag{A12}$$

For a given value of d/h, the solution for k_{II} and M is linear in S and τ. Coefficients can therefore be introduced according to

$$k_{II}h^{-1/2} = C_k^\tau(d/h)\tau + C_k^S(d/h)S \tag{A13}$$

and

$$Mh^{-2} = C_M^\tau(d/h)\tau + C_M^S(d/h)S. \tag{A14}$$

These coefficients are plotted in Fig. A1 and are tabulated in Table 1. Assuming $S > 0$ and $\tau > 0$, the solution is only valid if the following side conditions are met: (i) $\sigma_{yy} < 0$ on $0 < x < d$; (ii) $\delta_y(x) > 0$ on $x < 0$; and (iii) $\delta_x(x) < 0$ on $0 < x < d$ with k_{II}. These side conditions place constraints on the range of S and τ. A careful examination of the solution provides the range of τ/S for which all auxiliary conditions are met; this range is plotted in Fig. A2. For $d/h < 1.5$ the condition first violated is (iii) with k_{II} becoming positive; for $d/h > 1.5$, σ_{yy} becomes positive for values of x slightly smaller than d when the boundary in Fig. A2 is crossed.

A plot of the results from Table 1 in the form $\mathscr{G}_{tip}/\mathscr{G}$ [equations (8) and (10)] against τ/S, for fixed d/h, reveals that a good approximation in the range $0.2 \leqslant \mathscr{G}_{tip}/\mathscr{G} \leqslant 1$ is

$$2\mathscr{G}_{tip}/\mathscr{G} \cong 1 - C(d/h)\tau/S \tag{A15}$$

where $C(d/h)$ is plotted in Fig. A1(a). This formula was useful in computing the results plotted in Fig. 11.

Finally, it can be mentioned that a consistency check on the solution can be obtained with the aid of the J-integral as

$$\frac{(1-\nu^2)}{2E}[S^2h + 12M^2h^{-3}] = -\tau\delta_x(0) + \frac{(1-\nu^2)}{E}K_{II}^2. \tag{A16}$$

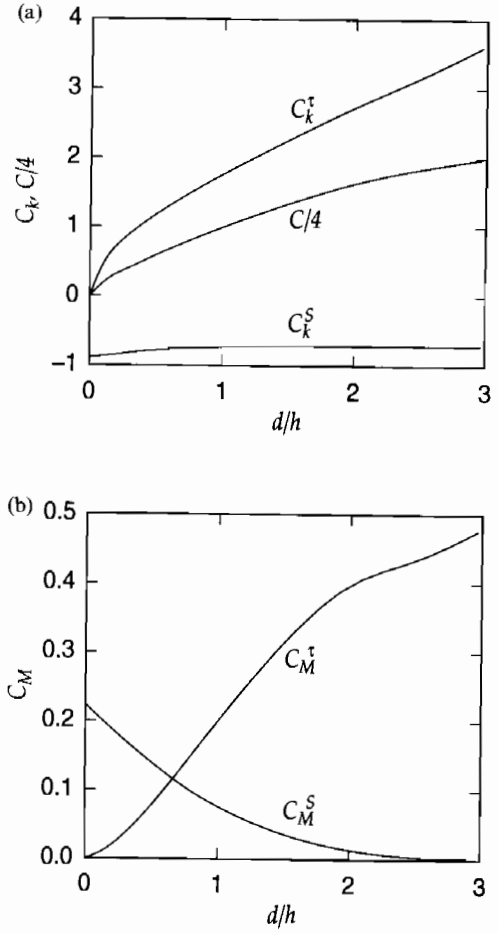

Fig. A1. Coefficients of τ and S in equations for k_{II} and M.

Table 1. Coefficients of τ and S in equations for k_{II} and M

d/h	C_k^τ	C_k^S	C_M^τ	C_M^S	C
0.00	0.00	−0.89	0.00	0.224	0.00
0.10	0.51	−0.87	0.006	0.205	0.80
0.20	0.73	−0.85	0.019	0.188	1.3
0.30	0.90	−0.82	0.035	0.171	1.6
0.50	1.19	−0.78	0.076	0.139	2.4
0.75	1.49	−0.75	0.138	0.103	3.2
1.00	1.77	−0.73	0.202	0.074	4.0
1.50	2.27	−0.71	0.32	0.033	5.4
2.00	2.75	−0.71	0.41	0.012	6.6
2.50	3.15	−0.71	0.43	0.003	7.4
3.00	3.64	−0.71	0.48	0.001	8.0

If one imagines an incremental advance of the crack with S, M and τ all held fixed, this equation states that part of the total energy released (the left-hand side of the equation) goes into frictional sliding and the remainder is released at the crack tip.

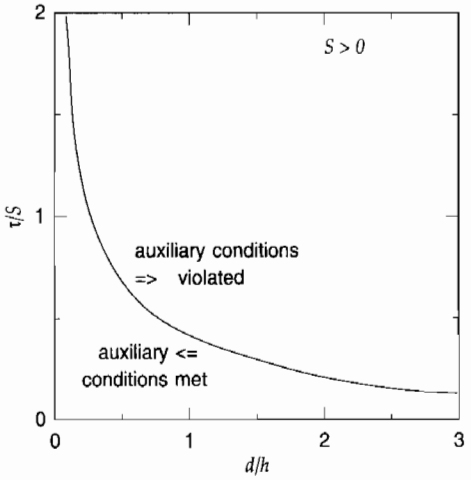

Fig. A2. Plot of τ/S against d/h showing where the auxiliary conditions are met or violated.